Null Power Reallocation for Data Rate Improvement in a Wireless Multicarrier System

by

Yun Wu

Submitted to the Department of Electrical Engineering and Computer Science
in partial fulfillment of the requirements for the degree of

Master of Engineering in Electrical Engineering and Computer Science

at the

MASSACHUSETTS INSTITUTE OF TECHNOLOGY

August 2007

Author .....
Department of Electrical Engineering and Computer Science
August 31, 2007

Certified by ..
Charles G. Sodini
Professor, Electrical Engineering and Computer Science
Thesis Supervisor

Accepted by .....
Arthur C. Smith
Chairman, Department Committee on Graduate Students

Null Power Reallocation for Data Rate Improvement in a Wireless Multicarrier System

by

Yun Wu

Submitted to the Department of Electrical Engineering and Computer Science
on August 31, 2007, in partial fulfillment of the
requirements for the degree of
Master of Engineering in Electrical Engineering and Computer Science

Abstract

Multicarrier systems are advantageous for high data rate transmissions in wireless environments due to their ease of implementation and tolerance for multipath delay spread. Currently, these systems as specified by the IEEE 802.11 standards do not adapt to frequency-selective fading but simply choose a constant data modulation scheme and transmit power level for all subcarriers in the available signal bandwidth. Although these implementations maintain acceptable performance when channel conditions are poor, they do not efficiently utilize the full capacity of a transmission channel. In the prototype system of the Wireless Gigabit Local Area Network (WiGLAN) project at MIT, a more efficient scheme is demonstrated where the modulation scheme of each subcarrier is selected individually based on the Signal-to-Noise ratio (SNR). To further improve the data rate of the WiGLAN system, this thesis describes the design of an adaptive transmit power allocation scheme that involves redistributing the power of "null" subcarriers with extremely low SNRs to the subcarriers that are utilized for data transmission. Experimental results demonstrate functionality of the simple redistribution scheme using the prototype transceiver nodes over various wireless channels, and show an average data rate improvement of 4.38% when the redistribution power is provided by 8 null subcarriers. Furthermore, a higher-complexity waterfilling redistribution scheme is simulated and compared against the simple redistribution scheme. The simulations of the waterfilling scheme predict a higher data rate increase of 13.2% over no redistribution if given the same power availability of 8 null subcarriers.

Thesis Supervisor: Charles G. Sodini
Title: Professor, Electrical Engineering and Computer Science

Acknowledgments

First I would like to thank my advisor, Prof. Charles Sodini, for giving me the opportunity to work on this project and guiding me through it. I appreciate Charlie's dedication and will remember him as a source of inspiration.

I would like to thank Prof. Dina Katabi for her unique perspective and suggestions during meetings with the WiGLAN group. Also, I would like to thank Prof. Anantha Chandrakasan for his inspiring class in digital systems, and I would like to thank Prof. Joel Schindall for his helpful professional advice.

I would like to thank all of the students past and present who have been involved in the WiGLAN project and have made my work possible. I would like to thank Farinaz Edalat for helping me get started and for always taking the time to answer my questions. I would like to thank Hariharan Rahul for teaching me about the software and PCI, and for sharing the computer. I would like to thank Khoa Nguyen for teaching me about the hardware and helping with the debugging. I would like to thank Jit Ken Tan for his thesis and previous work, and I would like to thank Nir Matalon for his work on the hardware.

I would like to thank the other members of the Sodini/Lee groups for the unique lab environment and friendships: Matt Guyton, Mariana Markova, SungAh Lee, Ivan Nausieda, David He, Mark Spaeth, Soonkyun Shin, Johnna Powell, Jack Chu, Kevin Ryu, Ke Lu, John Fiorenza, Albert Chow, and Jeff Feng. Also, I would like to thank Rhonda Maynard for her invaluable administrative support.

Lastly, I would like to thank my friends and family for the moral support and amazing college/grad school experience over the past five years: Mimi Xue, Yiyan Jiang, Tiffany Kosolcharoen, Lynn Ngo, Lisa Chen, Brian Hemond, Dmitry Malioutov, Ning Wu, Jim Sukha, and Lynne Salameh. Finally, and most importantly, I would like to thank my parents - my dad for always being patient and encouraging me in engineering, and my mom for her love, honesty, and optimism.

This work was funded in part by the MIT Center for Integrated Circuits and Systems.

Contents

List of Figures

List of Tables

Chapter 1

Introduction

In recent years, the demand for reliable high data rate wireless services such as multimedia broadcasting and file transfer applications has caused research in multicarrier communication systems to grow [1]. In a multicarrier system, a high rate data stream is partitioned into a set of lower rate streams that are transmitted in parallel by a set of subcarriers [2]. For wireless environments, the multicarrier system is more advantageous than the single carrier system because it is more robust and easier to implement. Compared to a high rate data stream transmitted by the single carrier system, lower rate streams transmitted by the multicarrier system have longer signal durations, so they are more tolerant of multipath interference as well as timing synchronization offsets between the transmitter and receiver [3]. Additionally, multicarrier systems are easier to implement because they partition a wideband frequency selective channel into a set of flat-fading narrowband channels and eliminate the need for complex equalization at the receiver to correct for frequency selective fading.

Multicarrier systems often choose from one of several data rates or modulations to use when transmitting data depending on the current channel conditions. For the best overall network performance, data should be transmitted using the highest possible modulation [4]. However, the current implementations as specified by the IEEE 802.11 standards do not adapt to fading conditions present in wireless environments, but simply choose a constant data modulation scheme across all subcarriers in the system and evenly allocate transmit power among the subcarriers. Although these

implementations are effectively designed for the worst-case channel conditions, they do not efficiently utilize the full capacity of the channel.

The WiGLAN research project at MIT has demonstrated a more efficient channel utilization scheme in a prototype transceiver system [5]. In the current implementation, the transmitter adapts the modulation of each subchannel individually when sending data. Compared to choosing uniform modulation across all subchannels, adapting modulation on a per-subcarrier basis can allow for a desirable increase in data rate or decrease in bit error rate. However, the current implementation does not adaptively allocate transmit power but simply distributes it evenly among all the subcarriers. In this thesis, an adaptive transmit power scheme is implemented for the current WiGLAN transceiver to further improve its performance. The performance of this simple redistribution scheme is analyzed through simulations and demonstrated with experimental results. Additionally, a more sophisticated waterfilling power redistribution scheme is developed in simulation, and its expected performance in hardware is predicted.

1.1 Outline of Thesis

The remainder of this thesis is organized as follows. In Chapter 2, background information in multicarrier communications is provided and an overview of the WiGLAN transceiver is presented. Chapter 3 describes the implementation of a simple adaptive transmit power allocation scheme, and provides simulation and experimental results assessing its performance. In Chapter 4, simulation results of a more sophisticated waterfilling power redistribution scheme are presented and compared against the actual hardware performance of the simple allocation scheme. Chapter 5 draws conclusions and provides suggestions for future work.

Chapter 2

WiGLAN Project Overview

As mobile file transfer becomes widespread, and as file sizes continue to expand, the push for increasing the data rate in Wireless Local Area Networks (WLANs) continues. At MIT, the goal of the Wireless Gigabit Local Area Network (WiGLAN) research project is to use prototype transceivers to conduct indoor channel experiments and demonstrate data rates of up to 1 Gbps [6]. In the following sections, the multicarrier communication principles used in the WiGLAN transceiver are explained and an overview of the prototype design is provided. The purpose of this chapter is to provide background for understanding the current prototype system and its capabilities.

2.1 Multicarrier Communications

Multicarrier modulation is a physical layer technique used to overcome the distortions impacting data transmission in wireless environments such as time delay spread, attenuation in signal strength, and frequency broadening [7]. These distortions are caused by reflections generated when a transmitted data signal runs into objects in its path, as shown in Figure 2-1. As a result, the signal received is the sum of multiple reflected signals. This reflection of multiple transmission paths at the receiver is known as multipath.

In Section 2.1.1 the wireless channel model used to predict the effects of multipath

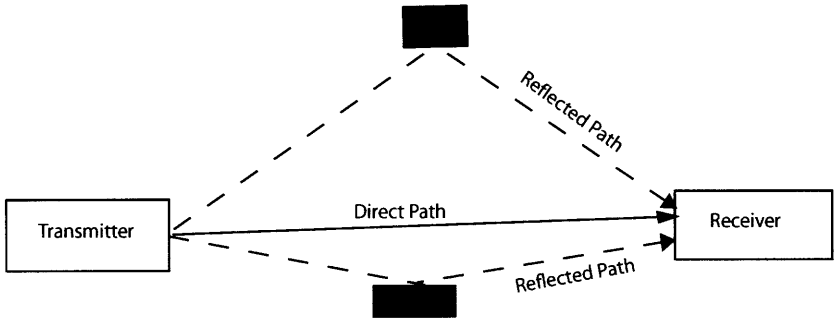

Figure 2-1: Multipath Scattering in a Wireless Environment

on a transmitted signal is presented. Following Section 2.1.1, Section 2.1.2 describes the principle of Orthogonal Frequency Division Multiplexing, a common multicarrier technique used to achieve high data rates and combat the effects of multipath fading in wireless communications. Finally, modulation types are described in Section 2.1.3.

2.1.1 Wireless Indoor Channel Model

For a wireless environment, the combined effects of the multipath transmission channel can be approximated by a finite impulse response (FIR) filter with time varying taps [7]:

$$c(\tau, t) = \sum_n \alpha_n(\tau_n(t)) e^{-j2\pi f_D \tau_n(t)} \delta[t - \tau_n(t)] \tag{2.1}$$

where

- $c(\tau, t)$ is the response of the channel at time t when an impulse is applied at time $t - \tau_n(t)$
- $\alpha_n(t)$ is the attenuation of the nth path
- $\tau_n(t)$ is the propagation delay for the nth path
- f_D is the Doppler shift for the signal received on the nth path

The received signal energy can be determined by taking the magnitude of the channel impulse response squared [8]:

$$P(\tau, t) = |c(\tau, t)|^2 \tag{2.2}$$

Multipath spread, usually denoted as T_m, can be quantified using rms delay spread, mean excess spread, or maximum excess delay. In the WiGLAN system, multipath spread is quantified using the maximum excess delay parameter. Maximum excess delay is defined as the time interval required for the received signal energy to fall below X dB of the strongest arriving signal [8]. In the WiGLAN system, X is chosen by determining the maximum amount of noise the system can tolerate with its highest modulation scheme without compromising the bit error rate, and is set to 32.31 dB. Therefore, if $\tau_0(t)$ is the time of the first arriving signal, and $\tau_x(t)$ is the maximum delay at which a multipath component is within X dB of the strongest arriving signal, which doesn't necessarily arrive at $\tau_0(t)$, then:

$$T_m = \tau_x(t) - \tau_0(t) \tag{2.3}$$

Coherence bandwidth B_m is also a measure of the multipath spread of the channel, and is defined as [8]:

$$B_m = \frac{1}{2\pi T_m} \tag{2.4}$$

where T_m is the multipath spread. If a transmit signal has a bandwidth that is smaller than the coherence bandwidth of the channel, then it will experience frequency non-selective fading as it passes through the channel. In the indoor environment used for testing the prototype WiGLAN transceivers, T_m is 70 ns and B_m is approximately 2 MHz [6].

Generally, indoor environments are characterized by slowly fading frequency selective channels [7]. A slowly fading channel has properties that do not change rapidly and remain fairly constant over several symbol intervals. A frequency-selective channel will distort a signal by adding different amounts of attenuation to different fre-

quency components of the signal. In order to recover a signal that has passed through a frequency selective channel, a complex multi-tap equalizer is required at the receiver. However, if the wideband frequency selective channel can be partitioned into several independent frequency non-selective narrowband subchannels, then the subcarrier signal within each subchannel will experience the same amount of attenuation across all of its frequency components, and a complex equalizer is no longer required. This partitioning process can be accomplished through Orthogonal Frequency Division Multiplexing and is described in the following subsection.

2.1.2 Orthogonal Frequency Division Multiplexing

In Orthogonal Frequency Division Multiplexing (OFDM), an entire wideband channel is partitioned into a set of subchannels, and the aggregate sum of the subchannels is transmitted [3]. The main principle of OFDM is to divide the channel into as many subchannels as possible to allow for the greatest spectral efficiency, yet choose the subchannels such that they are independent and only affected by Additive White Gaussian Noise (AWGN) but not affected by each other. Essentially, independent orthogonal subchannels are produced by using the Inverse Discrete Fourier Transform (IDFT) to process the data prior to transmission [9]. In the ideal case, the receiver recovers the original data using the Discrete Fourier Transform (DFT) operation. Generally, OFDM systems use N-point IDFT and DFT modules, and N is the number of input data samples that make up an OFDM symbol. A transform module processes N data samples in one "block" to produce N outputs. In order for the subcarriers to not interfere with each other during detection, it is shown in [7] that the spacing between the subcarriers must be at least $1/T$, where T is the time duration of N data samples.

Additionally, to achieve correct channel partitioning in OFDM, a block of samples known as the cyclic prefix (CP) must be inserted before each data symbol at the transmitter after the IDFT and removed prior to the DFT operation [10]. The samples used in the cyclic prefix correspond to the last v samples of that data symbol of N samples, where v is one less than the number of taps in the channel impulse

response [9]. Essentially, inserting a CP prior to transmission changes a linear channel convolution operation into a circular convolution operation, and also spaces the data symbols far enough apart to avoid intersymbol interference (ISI). For a precise derivation of OFDM channel partitioning and the insertion of the CP in matrix form, please refer to [9].

In summary, OFDM uses the DFT and IDFT to partition a wideband channel into independent additive white Gaussian noise channels. In order to correctly achieve the partitioning, a cyclic prefix where the last samples of an OFDM data symbol is appended to the beginning of the symbol. In practice, the cyclic prefix adds slight performance degradation to the system but greatly simplifies the implementation of the channel partitioning. Additionally, the DFT and IDFT blocks are generally implemented using the Fast Fourier Transform (FFT) and Inverse Fast Fourier Transform (IFFT) for greater efficiency. These blocks allow the entire flow of data processing to be serialized and pipelined, so there is no time gap between the processing of successive data blocks.

2.1.3 Modulation Types

A multicarrier transmitter must perform modulation to map data bits into an analog form to send over the channel [7]. For an OFDM system, modulation can be done by changing the amplitude and phase of the transmitted RF carrier signal. Amplitude Shift Keying (ASK) modulations such as 2-ASK, 4-ASK, and 8-ASK transmit information by changing the amplitude of the carrier only, while Phase Shift Keying (PSK) modulations such as Binary Phase Shift Keying (BPSK) and Quadrature Phase Shift Keying (QPSK) transmit information by keeping the amplitude constant and changing the phase [11]. Finally, Quadrature Amplitude Modulation (QAM) schemes such as 4-QAM, 16-QAM, 64-QAM, and 256-QAM change both the amplitude and the phase of the carrier. All of these schemes are known as coherent modulations because they require the receiver to have knowledge of the modulation scheme used in order to demodulate the signal correctly and retrieve the bits. Although coherent modulation schemes require more complex receiver structures compared to non-coherent

Table 2.1: Number of Bits Encoded Per Subcarrier by Common Modulation Schemes

Modulation	*Bits Encoded (B)*
BPSK	1
QPSK	2
4-QAM	2
16-QAM	4
64-QAM	6
256-QAM	8

schemes, they are generally used because of their capacity for higher data rates for a given bandwidth.

The main decisions made by an OFDM system are the number of bits to transmit and the modulation scheme to use for each subchannel [7]. Generally, the higher the signal-to-noise ratio of the transmission channel, the greater the number of bits that may be transmitted in each subchannel if the transmission maintains a bit error rate (BER) constraint. The number of bits that commonly used modulation schemes may encode is shown in Table 2.1.

Each encoding for a set of B bits may be represented as a point in a constellation diagram corresponding to that modulation scheme as shown in Figure 2-2. Higher modulation schemes that encode more bits must have more constellation points denoting all the possible encodings, so as a result the encodings or "points" must be spaced closer together when the average transmit power for each subchannel is kept constant [7]. In Figure 2-2, this spacing between adjacent points is indicated as d. The smaller d in higher modulations means that the encoded signals are more similar to each other in terms of the modulated amplitude and phase, and thus require finer level differentiation at the receiver. As a result, higher modulations are more susceptible to channel noise which potentially generate bit errors. Therefore, the greater the amount of noise that is present in a channel, the lower the modulation and number of bits that can be sent and received correctly if a bit error rate constraint is satisfied.

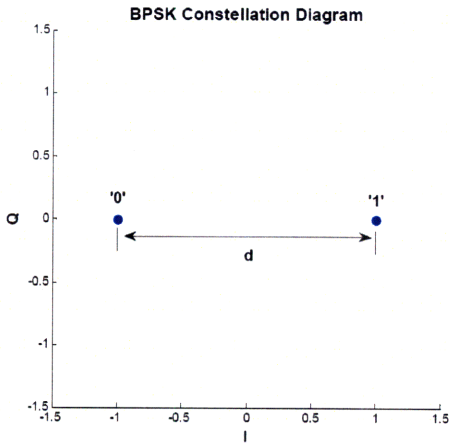

(a) BPSK

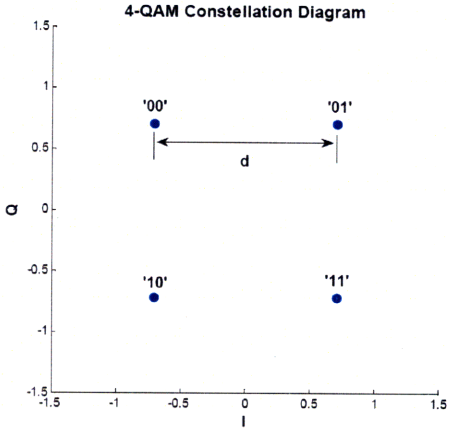

(b) 4-QAM

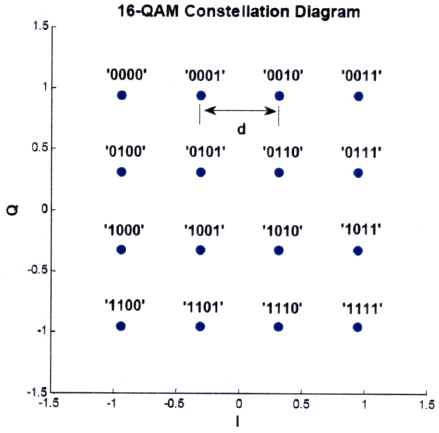

(c) 16-QAM

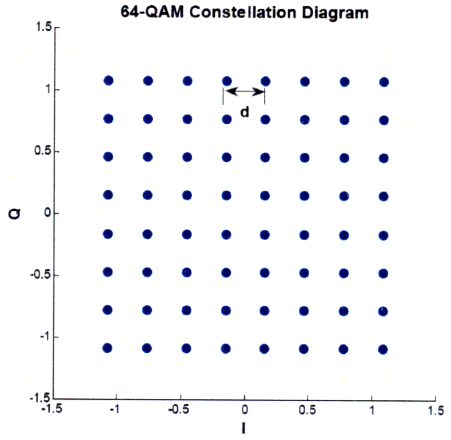

(d) 64-QAM

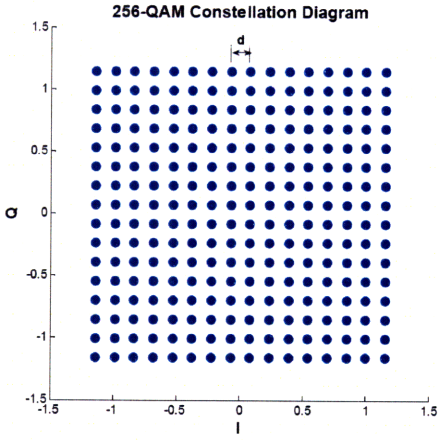

(e) 256-QAM

Figure 2-2: Constellation Diagrams With Same Average Power of 1 Unit

Table 2.2: Key Parameters of WiGLAN and 802.11a Systems

	WiGLAN	802.11*a*
Modulation Types	BPSK, 4-QAM, 16-QAM, 64-QAM, 256-QAM	BPSK, QPSK, 16-QAM, 64-QAM
Number of Data Subcarriers	92	48
Number of Pilot Subcarriers	8	4
Total OFDM Symbol Duration	1.4 μs	4 μs
CP Length	400 ns	800 ns
Subcarrier Spacing	1 MHz	0.3125 MHz
Signal Bandwidth	100 MHz	16.66 MHz
Channel Bandwidth	128 MHz	20 MHz
Carrier Frequency	5.25 GHz	5.25 GHz

2.2 The WiGLAN Node

Given the multipath characteristics of the wireless environment, the prototype WiGLAN nodes are designed to adapt to fading conditions and demonstrate higher channel utilization compared to 802.11a multicarrier systems [6]. Table 2.2 compares the specifications of the two systems. Both the WiGLAN system and the 802.11a system operate in the 5 GHz range, but the primary differences are the greater bandwidth and number of subcarriers used in the WiGLAN system [7]. With a wider bandwidth, the WiGLAN is able to achieve a higher data rate, but the variations among the subcarriers become more significant. In order to efficiently utilize the higher spectral capacity enabled by the wider bandwidth of the WiGLAN, frequency adaptive modulation and power redistribution are considered.

In the following subsections, the WiGLAN node is described. Section 2.2.1 summarizes the overall design of the transceiver, and Sections 2.2.2 and 2.2.3 summarize the design of the baseband transmitter and receiver implemented in the FPGA. Finally, Section 2.2.4 explains the current frequency adaptive modulation protocol used.

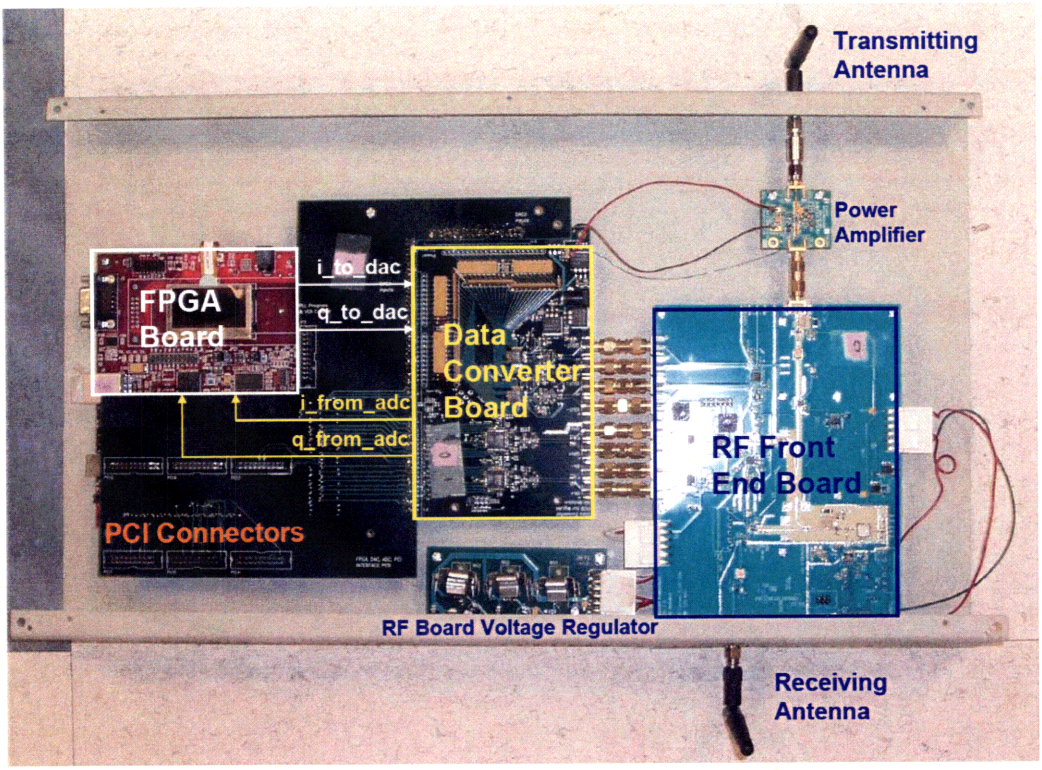

Figure 2-3: The WiGLAN Node

2.2.1 Overall Design

The WiGLAN transceiver node is shown in Figure 2-3, and can be divided into a baseband portion and a front end portion [6]. The baseband portion is implemented in a Xilinx Virtex4-XC4VSX35-10FF668 Field Programmable Gate Array (FPGA) mounted on a commercial Avnet Evaluation Board indicated as *FPGA Board* in Figure 2-3. The main functionalities of the baseband portion include performing adaptive data modulation and demodulation according to the OFDM principle of Section 2.1.2, accounting for signal degradation caused by non-idealities in the RF front end such as offsets between the RF carrier oscillators and sampling clock oscillators, and performing channel estimation and receiver packet detection [6].

The front end portion is documented in [12], and primarily consists of the custom made *Data Converter Board* and *RF Front End Board* as indicated in Figure 2-3. The data converter board includes two DACs and two ADCs to convert the

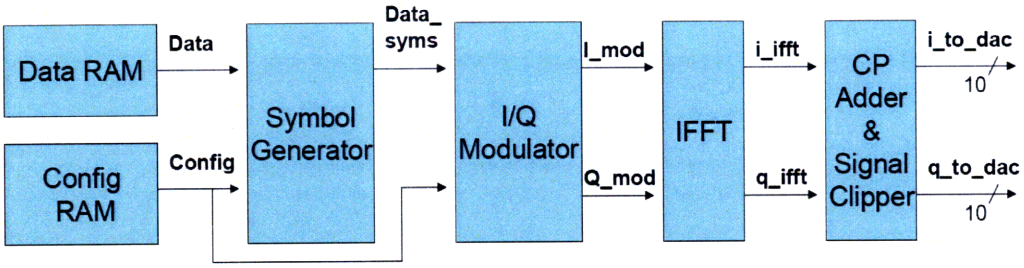

Figure 2-4: Baseband Transmitter Design

digital baseband signals into the analog domain for transmission by the RF board and the received analog signals back into the digital domain for processing by the FPGA board. The RF front end performs transmission and reception of wideband signals of up to 128 MHz bandwidth in the 5.247 GHz radio frequency band through the transmitting and receiving antennas. Finally, the node may be connected to a computer through the *PCI Connectors* allowing for more flexible data processing on a larger scale.

2.2.2 Baseband Transmitter

The block diagram of the WiGLAN transmitter is shown in Figure 2-4. The transmitter may obtain data from either an internal RAM inside the FPGA or from an external source fed in through the PCI connectors. The data and the corresponding modulation configuration are sent into the *Symbol Generator* which groups the data stream into symbols. Then the *I/Q Modulator* and *IFFT* blocks modulate and transform the data symbols into the time domain. Next, the *CP Adder and Signal Clipper* adds a cyclic prefix before each block of data and normalizes the amplitudes of the signals. Finally, the orthogonal data streams *i_to_dac* and *q_to_dac* are sent to the data converter board.

2.2.3 Baseband Receiver

In order for the WiGLAN system or any other multicarrier communications system to perform basic functions, the transmitter and receiver must be synchronized. To a large extent, synchronization abilities dictate the design of the receiver aside from the basic OFDM demodulator requirements. The OFDM receiver must detect the start of the packet, estimate and correct for a carrier frequency offset (CFO) and sampling frequency offset (SFO), and undo the effect of the channel. The overall block diagram of the receiver is shown in Figure 2-5. The basic receiver blocks that are required for reversing the operations of the OFDM transmitter are the *CP Remover*, *FFT*, *I/Q Demodulator* and *Symbol Parser*. Additionally the *SNR Estimator* estimates the signal-to-noise ratio of each subchannel, which is required for frequency adaptive modulation, and is described in more detail in 2.2.4. The remaining blocks that allow for synchronization and correction of nonidealities are described in the following subsections.

DC Offset Remover and Packet Detector

The performance of the detection algorithm used by the *Packet Detector* degrades when there is a large DC offset present in the received signal. Therefore the WiGLAN receiver uses a *DC Offset Remover* prior to the *Packet Detector* to remove this DC component. The drawback of the DC filter is that it causes slight degradation of subcarriers around the DC bin.

To detect the beginning of the received packet, the *Packet Detector* uses a double sliding window algorithm, as described in [7]. Two consecutive sliding windows of received energy of n samples each, a_n and b_n, are calculated, and their ratio m_n defined as a_n/b_n is computed. When both sliding windows contain only received noise, the ratio of the received energies in the two windows will remain constant. When the first window a_n begins to detect the packet, its received energy will increase relative to the second window, and the ratio m_n will increase. When this ratio crosses over a threshold value, packet detection is asserted. The peak of m_n corresponds to the

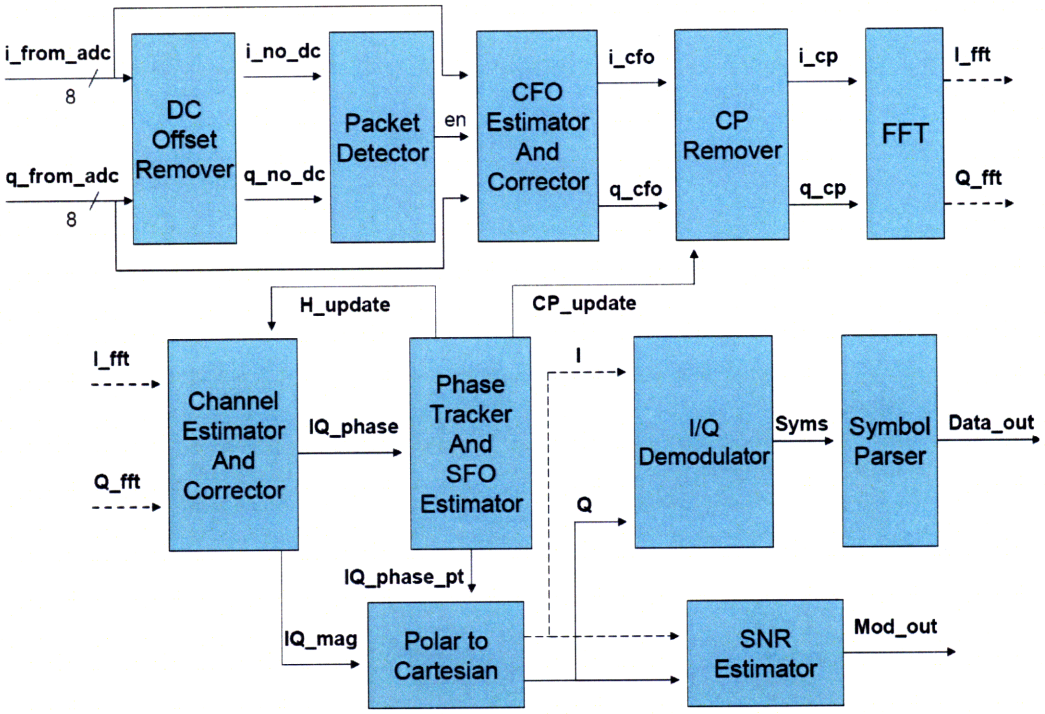

Figure 2-5: Baseband Receiver Design

point where sliding window a_n completely contains the packet and b_n contains only noise. The sample index n at the peak corresponds to the start of the packet.

Carrier Frequency Offset Estimator and Corrector

Carrier frequency offset (CFO) refers to the difference in frequency between the carrier oscillators on the transmitter and receiver. If not corrected for, the subcarriers will no longer be completely orthogonal to one another at the receiver and intercarrier interference (ICI) that can lead to significant SNR degradation will result. In the WiGLAN, a maximum CFO of 500kHz may be estimated and corrected for by the *CFO Estimator and Corrector*. Essentially, this estimation is done by taking the cross correlation of two identical training symbols in the preamble of the packet and obtaining the phase, as described in [6] and [7].

Channel Estimator and Corrector

Besides detecting the start of the packet and correcting for the CFO, the receiver must also undo the attenuation caused by the channel. This estimation is done by the *Channel Estimator and Corrector* block after the *CP Remover* and *FFT* blocks. The recovered symbols are divided by the known training symbols, and the effective attenuation due to the channel and noise is obtained for each subcarrier. In the WiGLAN implementation, the effect of the channel is averaged over two training symbols to obtain a more accurate estimation.

Phase Tracker and Sampling Frequency Offset Corrector

The offset between the oscillator clocks at the DAC and ADC will also cause SNR degradation if not corrected for by a sampling frequency offset (SFO) corrector. Essentially, the received signal will be sampled at slightly shifted points relative to the transmitted signal and this shift of the symbol timing point will result in a rotation of subcarriers and intercarrier interference [13]. The ICI resulting from the SFO is usually insignificant and can be ignored in OFDM systems. However, the rotation of subcarriers due to SFO as well as residue CFO must be corrected for by the *Phase*

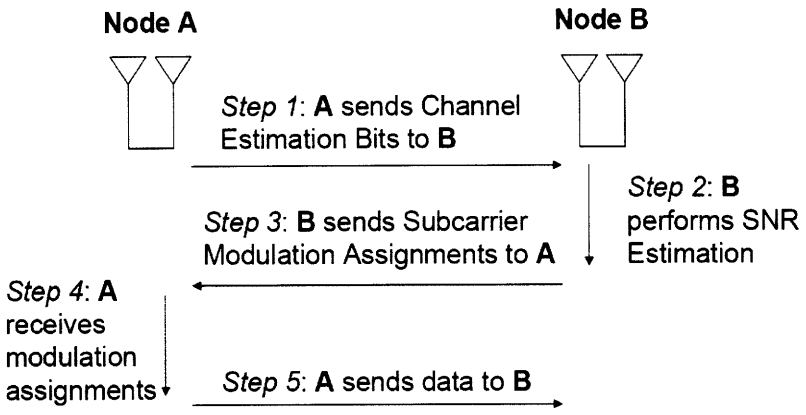

Figure 2-6: Frequency Adaptive Modulation Protocol

Tracker. Essentially the carrier phase tracking block performs a linear regression on eight received pilot data symbols that are sent at known frequencies and spaced evenly throughout the subcarriers in each OFDM, as described in [5] and [8]. After obtaining an updated phase, the magnitude and phase of the data streams are sent into a *Polar to Cartesian* conversion block, and the corrected I and Q data streams may then be demodulated and recovered by the *I/Q Demodulator* and *Symbol Parser*.

2.2.4 Frequency Adaptive Modulation

In the current WiGLAN system, the frequency adaptive modulation protocol improves upon conventional OFDM systems by selecting modulation on a bin-by-bin basis, as explained in [6]. To perform frequency adaptive modulation, channel state information (CSI) must be known and available to a transmitting node prior to data transmission. This information indicating the current conditions of the channel is determined by the receiving node and fed back to the transmitter in a five-step process as shown in Figure 2-6.

In Step 1, the transmitting node A sends a series of known training symbols to the receiving node B. Each training symbol consists of a set of 100 single data bits (0 or 1) modulated using BPSK and processed using the IFFT according to the OFDM

principle of Section 2.1.2. One data bit is sent in each subchannel so that the channel conditions can be estimated across the entire transmission bandwidth of 100 MHz used for the WiGLAN system. Node A repeatedly sends the same training symbol 37 times consecutively to allow for a more accurate averaged estimation of channel conditions by node B.

To estimate the channel conditions, node B compares the actual received data to the expected training symbols in Step 2, and quantifies the difference caused by channel noise using the Signal-to-Noise Ratio (SNR) metric. SNR is estimated as follows:

$$\widehat{SNR}_k = \frac{1}{\widehat{\sigma}_k^2} \tag{2.5}$$

$$\widehat{\sigma}_k^2 = \frac{1}{N}\sum_{i=1}^{N} |\widehat{X}_{i,k} - S_k|^2 \tag{2.6}$$

where

- N is the number of OFDM symbols used for the SNR estimation
- $\widehat{X}_{i,k}$ is the kth recovered sub-carrier data symbols for the ith symbol from the output of the OFDM receiver
- S_k is the training symbol for the kth subcarrier

After estimating the SNR, node B determines the appropriate modulation scheme (BPSK, 4-QAM, 16-QAM, 64-QAM, or 256-QAM) for each subchannel by checking the SNR against a set of thresholds. The thresholds levels are dependent on the target bit error rate of the system, and are chosen to allow for some margin in estimation error, as described in [6]. After assigning a modulation to each subchannel, node B returns the subcarrier modulation assignments to node A in Step 3. This information is sent back using the lowest modulation scheme (BPSK) and heavily coded to guard against errors. In Step 4, node A processes this received information indicating the appropriate modulation scheme to be used for each subchannel. Finally, in Step 5, node A modulates the actual data according to the modulation scheme and transmits the data to node B.

For the Frequency Adaptive Modulation protocol to work correctly, the entire five-step process must be completed within the coherence time of the channel before conditions have changed. For the WiGLAN project, it is assumed that continuous data transmission will not exceed 10 ms, which is well below the channel coherence time of 24 ms for essentially stationary transceiver nodes operating at a carrier frequency of 5.25 GHz. Additionally, regardless of the direction of data transmission, each node must be capable of both data transmission and reception at various stages in the five-step process. This progression through the five steps is dictated by controllers implemented as finite state machines in each node.

2.3 Summary

An overview of the prototype WiGLAN system and appropriate background information was presented in this chapter. In order to combat the effects of frequency selective fading in wireless environments as described in Section 2.1.1, the WiGLAN system uses a common channel partitioning method known as Orthogonal Frequency Division Multiplexing, as discussed in Section 2.1.2. Additionally, modulation types were discussed in Section 2.1.3 as background for understanding the frequency adaptive modulation scheme of the WiGLAN system described in Section 2.2.4. Finally, the overall design of the WiGLAN node as well as the implementations of the baseband transmitter and receiver were presented in Sections 2.2.1, 2.2.2, and 2.2.3 to serve as a basis for understanding the work of this thesis as described in the subsequent chapters.

Chapter 3

Simple Null Power Reallocation

In Chapter 2, an overview of the WiGLAN system was presented. The key characteristics of the prototype transceiver are its implementation of channel partitioning using Orthogonal Frequency Division Multiplexing and its use of a frequency adaptive modulation scheme. As shown in [6], adapting modulation on a per subcarrier basis allows for an improvement in data rate or a decrease in bit error rate compared to a standard 802.11a OFDM transceiver. However, to improve the capacity of the WiGLAN transceiver even further, transmit power can be more efficiently allocated under the frequency adaptive modulation scheme. Before power reallocation, the total power budget is uniformly distributed among 100 subcarriers, where 92 are used for transmitting data and 8 are used for transmitting pilot tones. However, during SNR estimation, if the SNRs of some data bins fall below the BPSK SNR threshold, then they are assigned to be null bins, and cannot be used for actual data transmission. In this case, the power originally allocated to the null bins can be reallocated to the usable bins. With higher transmit powers, these useable subcarriers achieve higher SNRs under the same channel conditions, so they can transmit using higher modulations. Therefore, the reallocation process can lead to an overall improvement in the data rate.

In Section 3.1, the concept of null power reallocation is presented. Section 3.2 describes the implementation of the simple power redistribution scheme for the transmitting and receiving nodes beyond the existing frequency adaptive modulation protocol

Table 3.1: Average Power of Constellations in Terms of Distance (d) Between Adjacent Points

Modulation	*Average Power*
BPSK	$0.25d^2$
4-QAM	$0.5d^2$
16-QAM	$2.5d^2$
64-QAM	$10.5d^2$
256-QAM	$42.5d^2$

of the WiGLAN system. In Sections 3.3 and 3.4, the functionality and performance of this simple power redistribution scheme is evaluated through simulation and demonstrated with experimental results taken from the WiGLAN transceiver nodes.

3.1 Concept

The transmit power level of a subcarrier when sending a specific encoding of data bits can be determined through its constellation diagram, as previously shown in Figure 2-2, where the distance between two adjacent points in a constellation is d. The power required to send a specific encoding is equal to the squared distance between the constellation point and the origin [14].

The average power for a constellation can be calculated by computing the squared distance between each point and the origin, and taking the average over all points in the constellation. Table 3.1 indicates this average power for each constellation in terms of d. In this reallocation scheme, the average power of each subchannel is normalized and considered as one unit during the baseband processing. The resulting d values for an average power of 1 are shown in Table 3.2. In simple null power redistribution, each null bin has 1 unit of power. The total power of all null bins is reallocated uniformly among the useable subcarriers, so their average transmit powers are increased. At the same time, the total transmit power level across all subcarriers remains the same because the null subcarriers now have zero units of power each. A greater average transmit power for a single useable subcarrier causes its constellation to essentially "expand". For a modulation upgrade to occur without causing an

Table 3.2: Resulting Distance Between Adjacent Points for Constellations of Average Transmit Power of 1 Unit

Modulation	*Normalized Distance (d)*
BPSK	2
4-QAM	1.414
16-QAM	0.632
64-QAM	0.309
256-QAM	0.153

Table 3.3: Units of Additional Power Required for a Modulation Upgrade Without Decreasing Distance (d) Between Adjacent Points

Modulation Upgrade	*Additional Power Required (units)*
BPSK to 4-QAM	1
4-QAM to 16-QAM	4
16-QAM to 64-QAM	3.2
64-QAM to 256-QAM	3.05

increase in the bit error rate, enough null power must be added so that the spacing between adjacent points d remains approximately the same. This additional null power requirement can be obtained by taking the ratios of average powers between consecutive modulations of Table 3.1 for a constant d, and subtracting off the one unit that represents the original unit of power in each subchannel. These results are shown in Table 3.3, and suggest that certain modulation upgrades are more likely to occur than others because they have a smaller additional power requirement amount.

In reality however, since each modulation tolerates a range of SNR and d values, a variable amount of power is required for a modulation upgrade depending on how close the SNR of that subcarrier falls to the SNR threshold of the next higher modulation scheme. Therefore, the power required for an upgrade may be significantly less than the worst case requirement shown in Table 3.3. This fact is explored in more detail in Section 4.1 of Chapter 4.

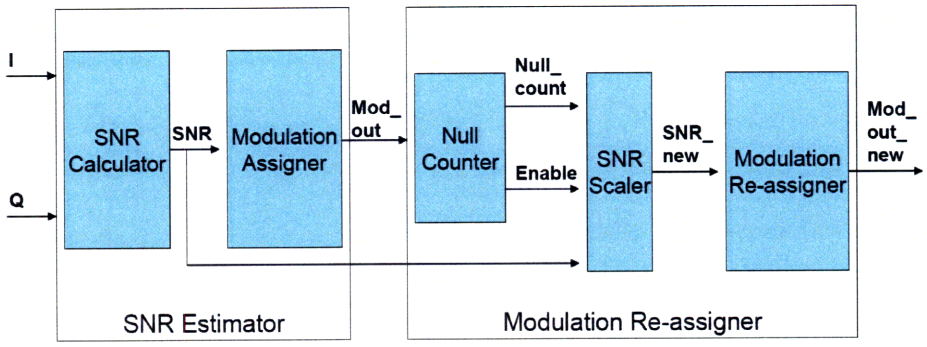

Figure 3-1: Simple Power Redistribution: Receiver Implementation

3.2 Implementation

3.2.1 Receiving Node

The receiver implementation of the simple power distribution scheme is shown in Figure 3-1. After the receiver performs SNR estimation in Step 2 as previously shown in Figure 2-6, the *Modulation Reassigner* of Figure 3-1 takes the old modulation scheme Mod_out, and counts the number of nulls. Based on the number of nulls, the *Modulation Reassigner* scales the old SNR by a precomputed scale factor stored in a ROM, redetermines the modulation based on the new SNR values SNR_new, and outputs a new modulation Mod_out_new.

The new Step 2 receiver implementation can substantially upgrade the modulation scheme if a significant number of nulls are counted. However, it requires one additional pass through the subcarriers, and adds a total of 138 clock cycles of latency to Step 2.

3.2.2 Transmitting Node

After the new modulation is fed back to the transmitter in Step 3 as shown in Figure 2-6, the transmitter may modulate data using the new scheme, but it must also successfully move the power from the null bins into the useable bins while keeping constant the average transmitter output power over the entire signal. In the sim-

ple distribution scheme, the extra power from the null bins is evenly spread among the useable bins, so the process of redistributing transmit power may be achieved by simply recounting the number of null bins, and increasing the amplitudes of the total transmit signal by multiplying by the appropriate scale factor. This amplitude scaling can be done either before or after the IFFT module of Figure 2-4. In this implementation, the latter scheme is chosen and incorporated within the Signal Clipper module. This module normalizes the amplitude of the time domain signal by scale factor f prior to transmission so that the average transmit power over the entire transmission signal is kept constant, and ensures that large peaks in the transmission signal that could saturate the data converters and cause bit errors will occur with a probability of less than 10^{-7}.

The appropriate amplitude scaling factor f for the transmit signal is chosen as follows. Given the i_{IFFT} and q_{IFFT} outputs of the IFFT module in Figure 2-4, the total signal can be represented as:

$$x_{IFFT} = \sqrt{i_{IFFT}^2 + q_{IFFT}^2} \tag{3.1}$$

The samples of x_{IFFT} make up a Gaussian distribution with zero mean and variance σ^2. Given such a Gaussian distribution, the error function $erf(x)$ can be used to determine the probability that a single instance of the distribution lies between $-c$ and c, where c is the clipping threshold. For the probability of a clip occurring in x_{IFFT} to be less than 10^{-7}, the proper clipping threshold c can be derived through probability theory, and the result is:

$$c = \sigma\sqrt{2} * erf^{-1}((1 - 10^{-7})^{\frac{1}{2N_{IFFT}}}) \tag{3.2}$$

$$\sigma = \sqrt{N_{USED}} \tag{3.3}$$

where N_{IFFT} is the number of samples that the IFFT module processes in one block, and N_{USED} is the number of subcarriers used. Therefore, x_{IFFT} will take on a larger range of values when N_{USED} is larger, and the clipping threshold c must increase

when N_{USED} increases to maintain a clipping probability of below 10^{-7}.

To normalize x_{IFFT} so that its average transmit power remains the same for any number of data subcarriers used, x_{IFFT} is multiplied by the scale factor f in the Signal Clipper module, where:

$$f = \frac{1}{c} \tag{3.4}$$

3.3 Simulation Performance

3.3.1 Proof of Concept

The functionality of the simple power redistribution scheme is assessed through simulation results gathered from Simulink. Compared to the original scheme that does not reallocate transmit power of null bins, this scheme allows for a variable increase in data rate that is highly dependent on the total number of null subcarriers for a given channel. In this section, the simulation is produced for an extreme scenario, where Additive White Gaussian Noise (AWGN) is added to the transmitted signal to produce 82 nulls out of 92 data subcarriers so that only 10 remaining subcarriers are useable for data transmission. The purpose of this section is to demonstrate the functionality of the power redistribution scheme, so for simplicity, the simulation does not incorporate a multipath channel model. The actual performance of the power distribution scheme under various multipath channels is assessed in Section 3.4.

The setup of the simulation is as follows. Two nearly-identical Simulink model files representing two transceiver nodes are simulated through a 5-step process as shown in Figure 2-6, where data values are generated into and supplied by a Matlab workspace. As already noted, AWGN is added to the transmitter output from Node A and fed into Node B without considering the multipath channel effects on the transmission signal. Additionally, the subcarrier modulation assignments fed back in Step 3 are assumed to be correct, as this information is heavily coded and sent using the lowest BPSK modulation.

Table 3.4: Effect of Power Redistribution on Modulation

	Normal	*After Power Redistribution*
Null	82	82
BPSK	10	0
4-QAM	0	10
16-QAM	0	0
64-QAM	0	0
256-QAM	0	0
Pilot	8	8
Total Subcarriers	100	100

Table 3.5: Normalized Average Baseband Transmitter Output Power During SNR Estimation and Data Transmission

	SNR Estimation	*Data Transmission*
Normal	0.050251	0.047997
Power Redistributed	0.050251	0.048218

Table 3.4 shows the resulting modulation distribution for the simulated channel with and without adaptive power redistribution. In this case, power redistribution of 82 null bins allows all 10 data carrying BPSK-modulated bins to be promoted to 4-QAM modulation. The new modulation scheme is sent back to the transmitting node in Step 3.

Table 3.5 compares the normalized average baseband transmitter output power of the SNR estimation in Step 1 with the output power during actual data transmission in Step 4. In both the normal and power redistributed implementations, the average power over the transmitted signal during data transmission does not exceed the average power used to send pilots during SNR estimation. This table shows that the baseband transmitter is indeed redistributing power to achieve a higher modulation scheme and not expecting the power amplifier to actually increase its average transmit power.

The final results of this 800000 clock cycle simulation are summarized Table 3.6. Within the 800000 cycle simulation, no bit errors were detected. Performing simple

Table 3.6: Data Bits Received in Normal and Power Redistributed Simulations

	Bits Received	*Data Rate (Bits/Symbol)*	*BER*
Normal	1888	10	-
Power Redistributed	3776	20	-

power redistribution for this hypothetical AWGN channel allows a doubling of the number of bits received and achieves a data rate improvement of 50%.

3.3.2 Realistic Simulation

In Section 3.3.1, the results of simple power redistribution are shown for a hypothetical AWGN channel that allow for a significant increase in data rate. However, for more realistic data, there are generally fewer available nulls and more diversity in the SNRs across subcarriers due to the effects of multipath. In this simulation, real SNR data previously gathered from hardware is fed directly into the *Modulation Assigner* block of the *SNR Estimator* of Figure 3-1. The simulation results are provided in Appendix A and predict that a hardware implementation of the simple redistribution scheme would lead to a data rate improvement of 4.48% if approximately 8 units of null power are available.

Figure 3-2 plots the Data Rate Increase vs. Number of Nulls for the simulated results. The plot shows that there is significant variability in the data rate improvement due to the nature of the simple redistribution algorithm. However, more nulls generally allow for a higher data rate increase percentage, as indicated by the line of best fit drawn through the point. Depending on the efficiency of the power redistribution algorithm, the slope of this trend line will vary. In this case, a increase in slope would correspond to an improved algorithm, where the same amount of null power achieves a more significant data rate increase.

The purpose of performing this realistic simulation is to establish a baseline for comparison when analyzing later results. In Section 3.4.2, the simple redistribution scheme is implemented in hardware, and experimental data is gathered and compared

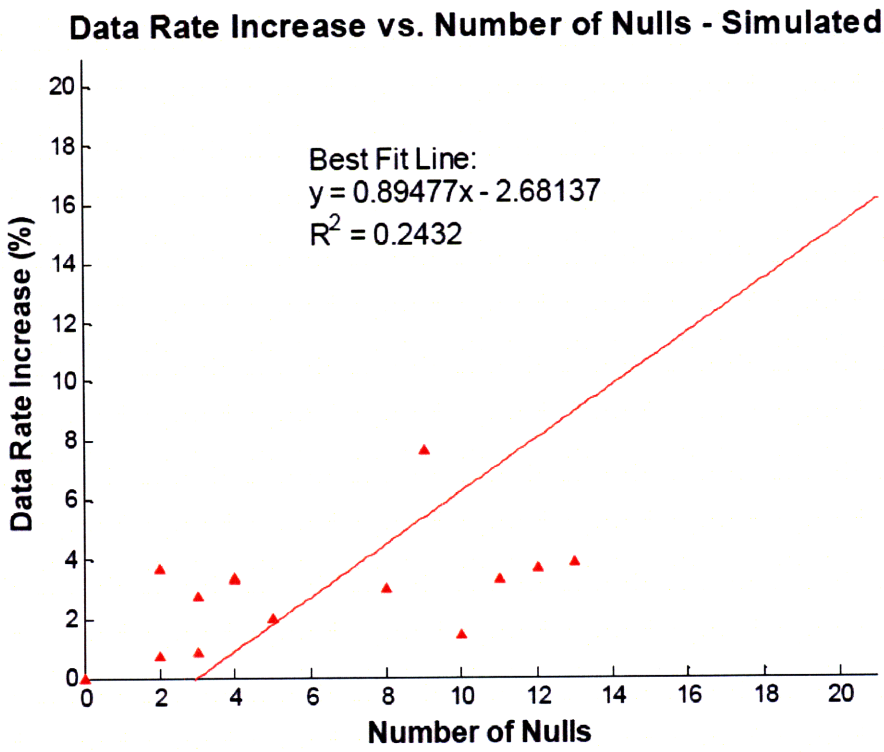

Figure 3-2: Data Rate Increase vs. Number of Nulls - Realistic Simulation

against this simulation to show that this simulation method accurately predicts actual performance. Later in Section 4.3, the same simulation method and the same set of SNR data are used to predict the performance of a waterfilling reallocation scheme.

3.4 Hardware Performance

The simple power redistribution scheme is implemented into the WiGLAN hardware and data is taken with various channel configurations, as described in Section 3.4.1. The experimental results provided in 3.4.2 show that generally there is diversity in the SNRs and modulation schemes across subcarriers due to the effects of multipath. Additionally, few nulls are usually available to provide power to be reallocated, and even in cases where a significant number of null bins are present, there are still large differences in the resulting data rate increase. On average, 8 nulls are present among 92 data subcarriers, and allow for a 4.38% increase in data rate when the null power is reallocated. All transmissions maintain a bit error rate of well below the target BER of 10^{-3}, and the average BER is $4.18 * 10^{-5}$ for each transmission of approximately 524,000 bits. Additionally, the hardware performance matches reasonably with the performance predicted by the realistic simulation of Section 3.3.2.

3.4.1 Experimental Setup

Data is taken with a pair of WiGLAN nodes for 7 different configurations in the MIT laboratory 38-229. Figure 3-3 shows the locations of the transmitting and receiving nodes. The location of the receiving node is fixed, while the location of the transmitter is varied within the reachable transmission vicinity of approximately 6.5 meters from the receiver, and is marked by the letters A through G in Figure 3-3.

The distances from the receiver and general quality of each channel configuration are given in Table 3.7. The channel quality is labeled as either line of sight (LOS) or non line of sight (NLOS). This simple categorizing is chosen because the main goal of the experiment is to assess the performance of the power redistribution scheme under realistic wireless channels, and not to rigorously assess or control the channel environ-

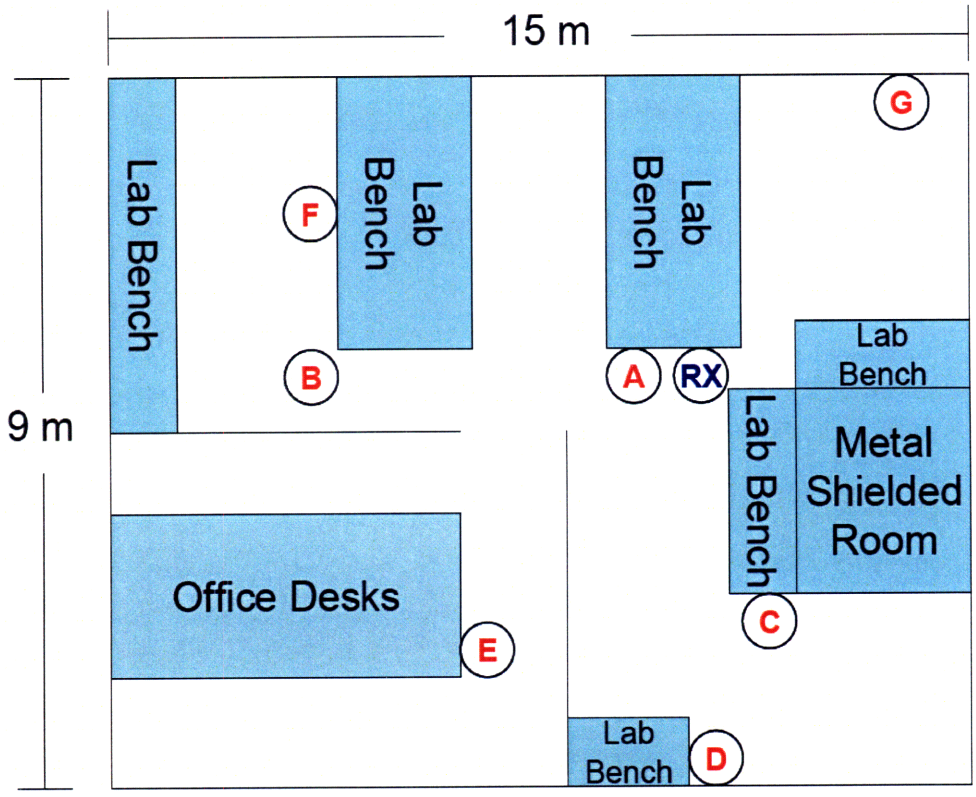

Figure 3-3: Locations of Receiving and Transmitting Nodes

Table 3.7: General Characteristics of Transmitter-Receiver Configurations

Transmitter Location	*Distance From Receiver (m)*	*Quality*
A	1.51	LOS
B	5.45	LOS
C	4.25	NLOS
D	6.35	LOS
E	5.35	NLOS
F	5.74	NLOS
G	3.79	NLOS

ment under each configuration. Approximately 7 trials are taken at each transmitter location, and data is considered valid for the cases where there are no errors in the Step 3 feedback data bits indicating the subcarrier modulation assignments. The following Section 3.4.2 summarizes the findings of the experiment, and this data is included in Appendix B.

3.4.2 Results

Figure 3-4 shows the overall effect of null power redistribution across locations A through G. The range of data rate increase is plotted, where each point indicates the average data rate increase of the location, and each bar shows the variability from one standard deviation below to one standard deviation above the average value. This figure shows that data rate increase due to null power redistribution does not simply depend on location, since the variability in data rate increase is extremely high across all locations. For example, in location F, variability ranges from close to zero up to 15%. The final column shows that when averaged over all valid trials, the simple null power redistribution scheme yields a 4.38% increase in data rate, but results within one standard deviation of the mean range from a 0.21% to 8.55% increase in data rate.

Figure 3-5 shows the effect of power redistribution on the overall modulation. Generally for all of the trials, most subcarriers have SNRs that fall within the 4-QAM and 16-QAM ranges. When power redistribution is implemented, the main

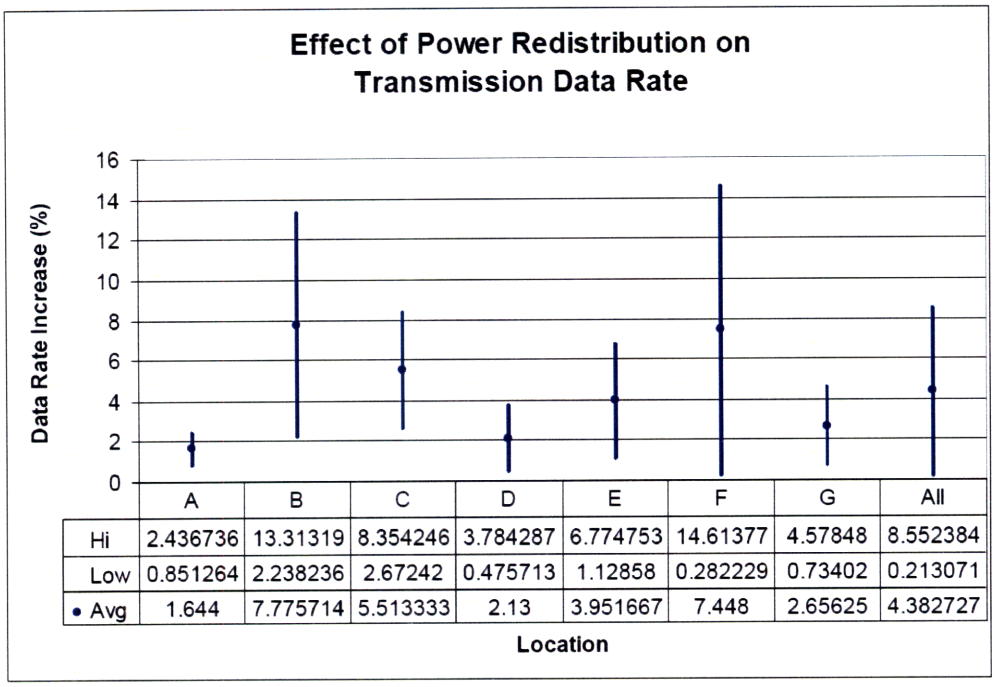

	A	B	C	D	E	F	G	All
Hi	2.436736	13.31319	8.354246	3.784287	6.774753	14.61377	4.57848	8.552384
Low	0.851264	2.238236	2.67242	0.475713	1.12858	0.282229	0.73402	0.213071
• Avg	1.644	7.775714	5.513333	2.13	3.951667	7.448	2.65625	4.382727

Figure 3-4: Effect of Power Redistribution on Transmission Data Rate

effects are an upgrading of subcarriers from BPSK to 4-QAM modulation, and an upgrading of subcarriers from 4-QAM to 16-QAM modulation. The overall result is an increase in the average number of bins modulated using 16-QAM, and a decrease in the average number of bins modulated using BPSK and 4-QAM.

Finally, Figure 3-6 plots the data rate increase percentage against the number of nulls for each valid trial and compares the actual data against the simulated results of Section 3.3.2. This figure shows that actual results of the simple power redistribution implementation match the simulated results very closely, and the best fit lines are almost identical when the number of nulls is below 10. Again, more nulls generally allow for a higher data rate increase percentage, and the efficiency of the redistribution algorithm is indicated by the slope of the linear regression line.

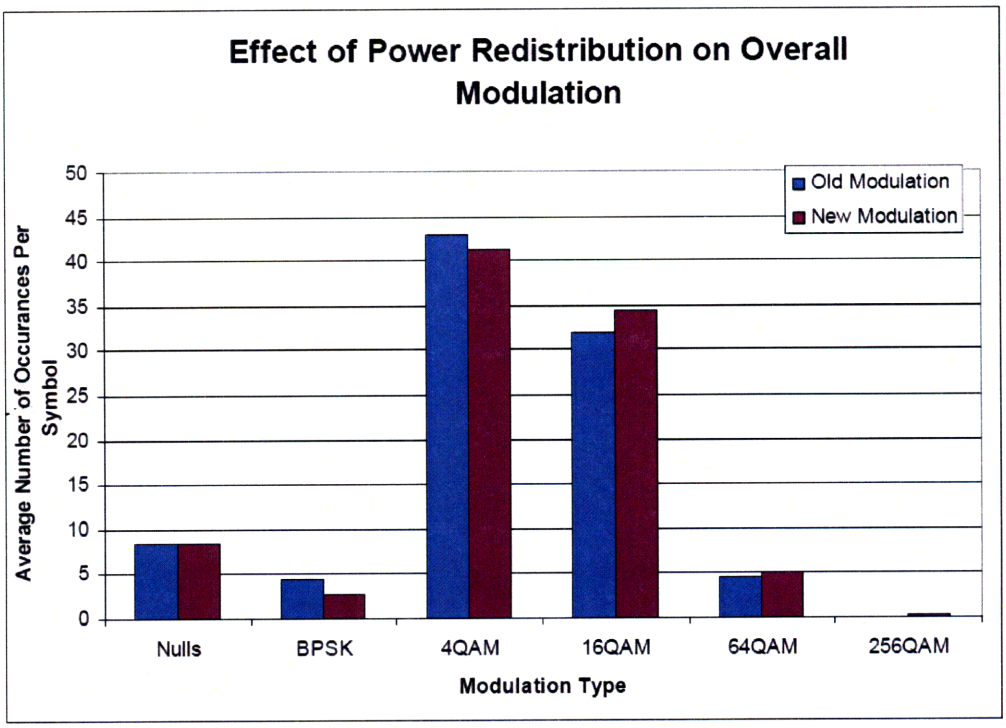

Figure 3-5: Effect of Power Redistribution on Overall Modulation

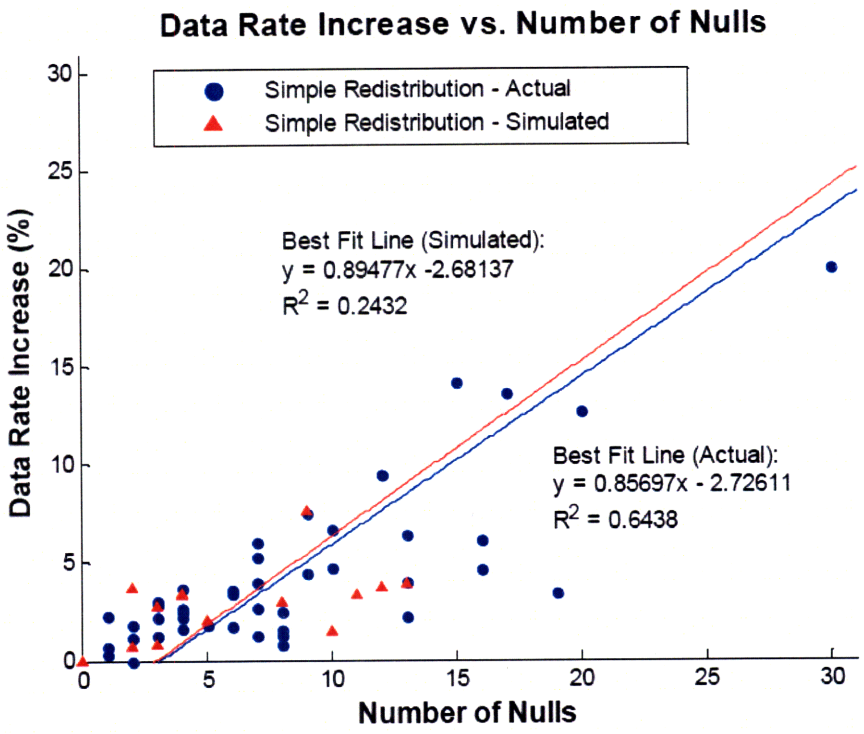

Figure 3-6: Data Rate Increase vs. Number of Nulls for Simple Power Redistribution

Chapter 4

Waterfilling Power Reallocation

In Chapter 3 a simple power reallocation scheme is designed such that the transmit power of null bins is reutilized by spreading the null power evenly among the useable bins. The overall performance of the simple reallocation scheme in hardware compared to the original data transmission scheme that does not consider transmit power reallocation is an average data rate increase of 4.38% given approximately 8 units of null power. However, the actual performance is highly variable even for a fixed number of nulls, and data rate improvement results within one standard deviation of the overall mean range from 0.21% to 8.55%.

To improve upon the simple allocation scheme, a more efficient null power distribution scheme is designed and analyzed in simulation. The key idea of the waterfilling power reallocation scheme described in this chapter is to selectively place the null power in the useable bins that have SNR values close to the upper thresholds of each modulation scheme. Instead of spreading null power evenly among all useable bins, this strategy only targets the bins that will guarantee an upgrade in modulation scheme when a given amount of null power is invested. The overall results achieved by the waterfilling reallocation algorithm in simulation are an increase in average data rate improvement and a decrease in performance variability compared to the simple reallocation scheme.

Section 4.1 describes the overall design of the waterfilling power reallocation algorithm, and Section 4.2 describes the implementations of the waterfilling receiver

and transmitter nodes. Finally, Section 4.3 assesses the performance of the waterfilling reallocation scheme in simulation and compares it to the results obtained for the simple reallocation scheme.

4.1 Overall Design

The main objective of the waterfilling reallocation is to selectively place null power into a few bins which are close to the SNR thresholds instead of evenly spreading the null power among all useable bins. Figure 4-1 shows the setup of the waterfilling scheme. Originally in Step 2 of Figure 2-6 the modulation of a subchannel is determined to be either Null, BPSK, 4-QAM, 16-QAM, 64-QAM, or 256-QAM depending on where the SNR of that subchannel falls. In the waterfilling approach, additional threshold levels are drawn in between the original threshold levels so that subcarriers with SNR values that fall within certain margins of the original threshold levels may be grouped together. The boundaries of these regions are defined by the additional power needed for a modulation upgrade, as also shown in Figure 4-1. By definition, each null bin contains 1 "unit" of power. All subcarriers with SNR values that fall in a region of Type A need at most 0.5 units of null power to be promoted to the next higher modulation. Those subcarriers with SNR values that fall in a Type B region can be promoted with 1 unit of power, and those subcarriers with SNR values that fall in a Type C region can be promote with 1.5 units of power. The waterfilling scheme does not consider allocating null power to subcarriers with SNR values that fall within the Type D regions because they are too far away from the threshold level of the next higher modulation. Additionally, Regions 1 and 16 are not considered. Region 1 subcarriers are already assigned the highest possible modulation, and Region 16 subcarriers make up the null bins that provide the reallocation power to begin with. For simplicity, this scheme does not consider promoting null subcarriers to BPSK modulation.

Additionally, these SNR regions are prioritized by the number of bits gained per unit of null power added, as indicated in Table 4.1. The subcarriers falling in Re-

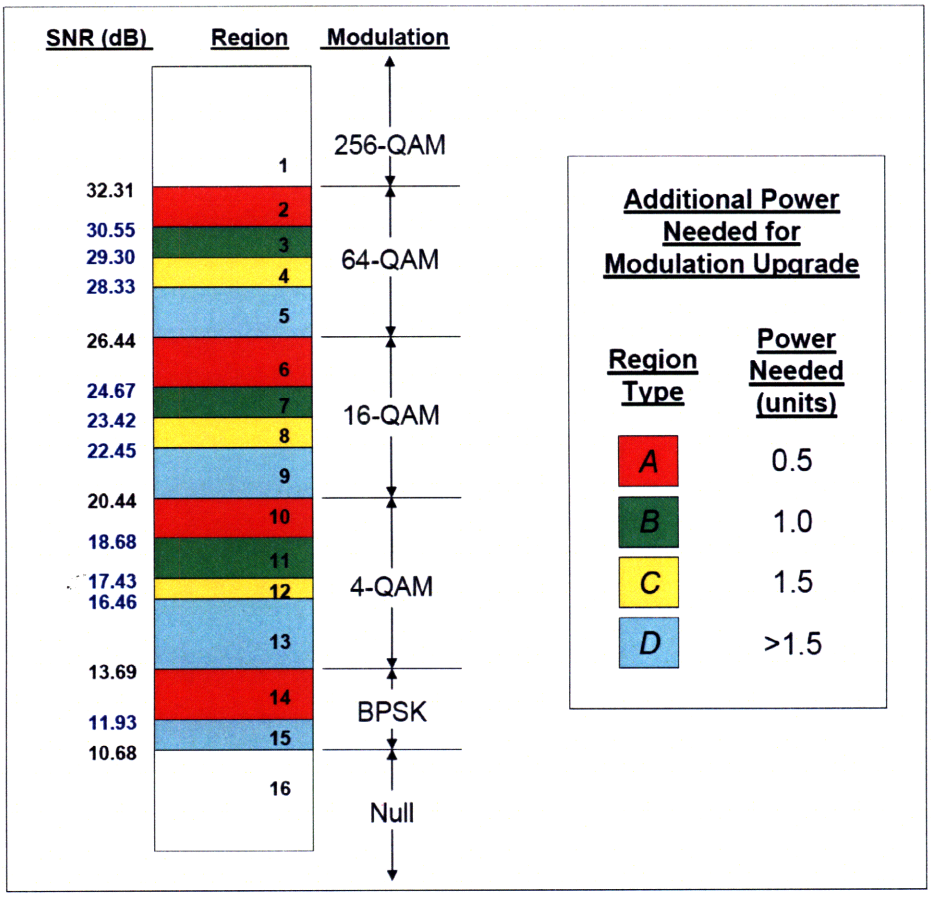

Figure 4-1: SNR Threshold Levels and Regions for Waterfilling Scheme

Table 4.1: Subcarrier Prioritization Based On Potential Number of Bits Gained Per Unit of Null Power Allocated

Region	*SNR Range (dB)*	*Bits Gained Per Unit Power Added*	*Priority*
1	> 32.31	N/A	None
2	30.55 to 32.31	4	I
3	29.30 to 30.55	2	II
4	28.33 to 29.30	1.33	III
5	26.44 to 28.33	< 1.33	None
6	24.67 to 26.44	4	I
7	23.42 to 24.67	2	II
8	22.45 to 23.42	1.33	III
9	20.44 to 22.45	< 1.33	None
10	18.68 to 20.44	4	I
11	17.43 to 18.68	2	II
12	16.46 to 17.43	1.33	III
13	13.69 to 16.46	< 1.33	None
14	11.93 to 13.69	2	II
15	10.68 to 11.93	< 2	None
16	< 10.68	N/A	None

gions 2, 6, and 10 have the highest number of bits gained per unit power added, so they are ranked Priority I and considered first. If there is still null power remaining after allocation to all Priority I subcarriers, then the receiver proceeds downward in a "waterfilling" manner, considering the Priority II subcarriers next. The receiver only considers Priority III subcarriers if there is still power remaining after "filling" the Priority I and Priority II subcarriers. This prioritization allows the implementation of the waterfilling receiver to be simplified. Instead of considering the SNR of each subcarrier individually when making power allocation decisions, the receiver may consider all subcarriers in one priority rank at once. The drawback of this simplification is a decrease in power allocation efficiency. In general, the greater number of priority levels defined, the more efficient the waterfilling algorithm will become. Additionally, since the null power resource is very limited in reality, it is unlikely that the receiver will have null power remaining after allocating power to all subcarriers in Priority III, so for simplicity, subcarriers past Priority III are not considered.

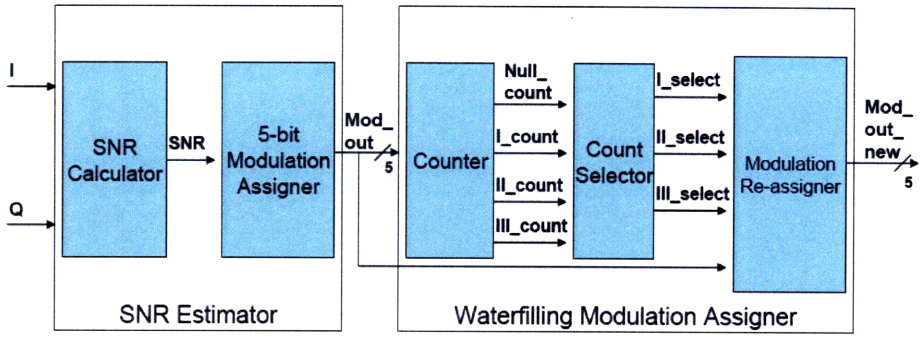

Figure 4-2: Waterfilling Power Redistribution: Receiver Implementation

4.2 Implementation

4.2.1 Receiving Node

The implementation of the waterfilling receiver is shown in Figure 4-2. This implementation is similar to that of the simple power redistribution implementation in that it only requires one additional pass through the 128 subcarriers in one symbol and adds a total of 141 clock cycles of latency to Step 2 in the five-step process of Figure 2-6. However, the *Modulation Assigner* inside the *SNR Estimator* is modified to consider the additional threshold levels described in Section 4.1, and now produces *Mod_out*, a 5-bit representation of the modulation type for each subcarrier. *Mod_out* is fed into *Counter* which not only counts nulls but also the number of subcarriers that fall under Priorities I, II, and III. These counts are fed into *Count Selector* which essentially performs the waterfilling. *Count Selector* takes the available null count and determines how many of the subcarriers falling under Priorities I, II, and III may actually be upgraded given the null power availability, and outputs the adjusted counts *I_select*, *II_select*, and *III_select* for the *Modulation Reassigner* block. The *Modulation Reassigner* adjusts the 5-bit *Mod_out* based on the adjusted counts and outputs a 5-bit *Mod_out_new* as the modulation assignment for each subcarrier. This modulation assignment information is sent back to the transmitting node in Step 3 of the five-step process.

4.2.2 Transmitting Node

After the modulation assignments are sent back to the transmitting node in Step 3, the transmitter may modulate data according to the new scheme. However, similar to the simple power redistribution implementation, it must also move power from the null bins to the targeted bins while keeping the average transmitter output power over the entire signal constant. However, since different amounts of power are now allocated to each subcarrier, the transmitter must scale the average power of each subcarrier by the appropriate factor in the frequency domain prior to the IFFT module instead of afterwards in the time domain. This scale factor is equal to the total power allocated for the subcarrier. Given that the waterfilling scheme assigns 0, 0.5, 1, or 1.5 units of additional power to each subchannel, the corresponding scale factors are 1, 1.5, 2, or 2.5.

4.3 Simulation Results

The performance of the waterfilling power redistribution scheme is assessed in simulation and compared to the simulation of the simple power redistribution scheme. Similar to the simulation of Section 3.3.2, the waterfilling simulation is set up so that real SNR data from hardware is fed directly into the *Modulation Assigner* inside the *SNR Estimator* block of Figure 4-2. The simulation results are provided in Appendix C. From these results, Figure 4-3 plots the Number of Nulls vs. Data Rate Increase and compares the waterfilling redistribution simulation to the simple redistribution simulation. For a given number of nulls, the waterfilling redistribution scheme achieves a higher data rate increase percentage, as indicated by the upper linear regression line. The regression line over the waterfilling simulation results predicts that given an average null power availability of 8 units, the waterfilling reallocation scheme would allow for a data rate improvement of 13.2%. This improvement is significantly higher than the data rate improvement of 4.48% predicted by the simple reallocation regression line for the same number of nulls.

Additionally, the performance of the waterfilling scheme in hardware will likely

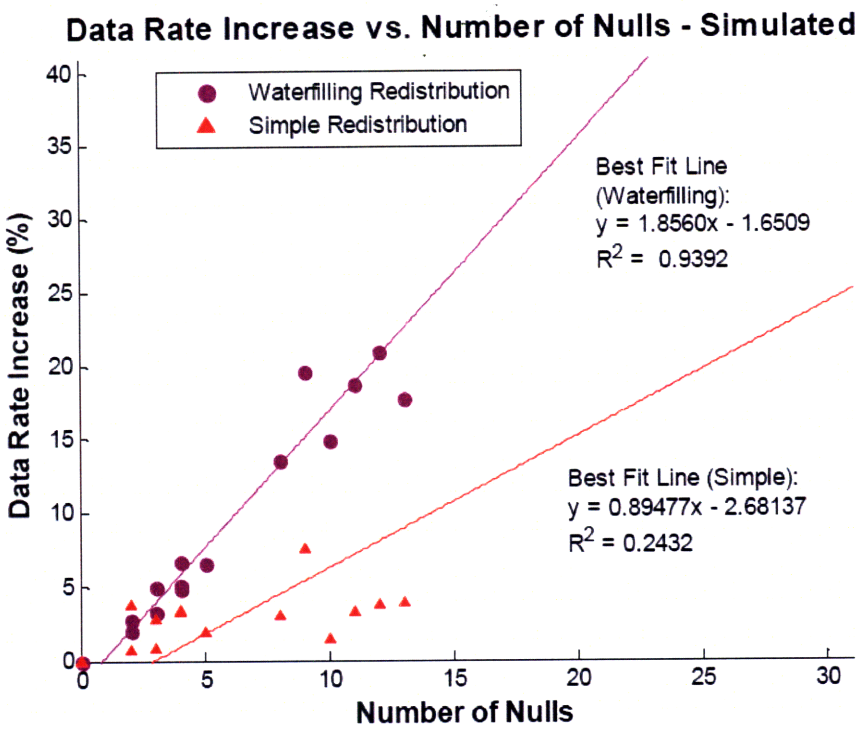

Figure 4-3: Data Rate Increase vs. Number of Nulls for Simple and Waterfilling Redistribution Schemes

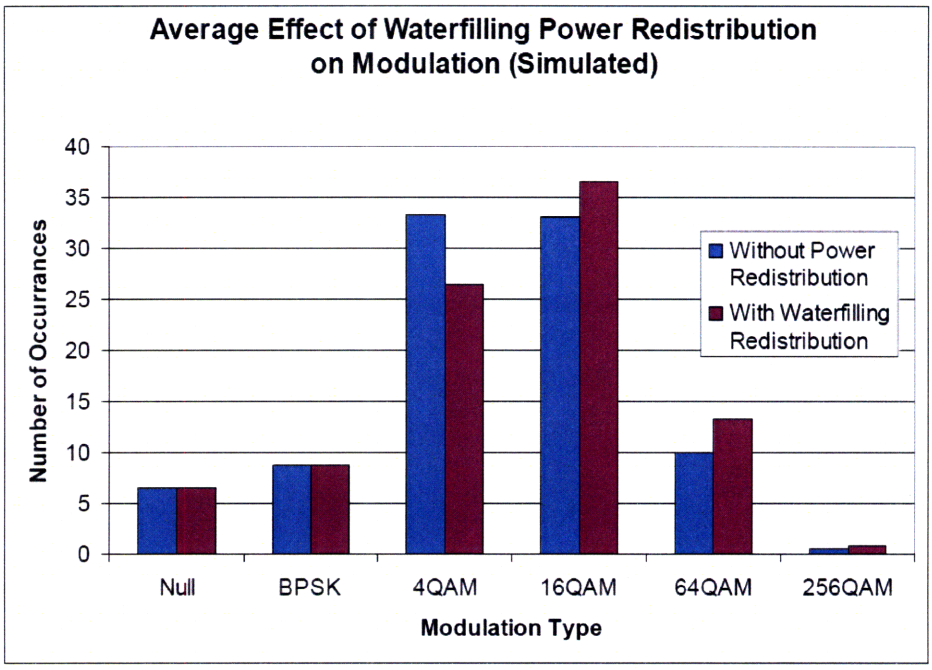

Figure 4-4: Average Effect of Waterfilling Power Redistribution on Modulation

yield a lower variance compared to the simple scheme because for a fixed number of nulls, the waterfilling scheme will target the power towards a few subcarriers that guarantee a fixed number of bits gained per unit of null power spent. Figure 4-4 shows the overall effect of the waterfilling simulation averaged over all results. Compared to the case where no null power redistribution is performed, the waterfilling scheme mostly allows 4-QAM and 16-QAM subcarriers to be promoted. The net result is a significant decrease in 4-QAM subcarriers and an increase in 16-QAM and 64-QAM subcarriers.

Chapter 5

Conclusion

5.1 Thesis Summary

This thesis described the implementation of a null power reallocation scheme for a multicarrier system, and assessed the performance of the scheme for the prototype WiGLAN system described in Chapter 2. Generally, the improvement in data rate due to null power redistribution is highly dependent on the number of null subcarriers in a given wireless channel. In Chapter 3, experimental results obtained with WiGLAN nodes in a laboratory setting showed that a simple null power reallocation led to an average data rate improvement of 4.38% for approximately 8 nulls. However, simply dividing null power equally among useable subcarriers also created high variability in the resulting data rate increase. In Chapter 4, implementation of a more sophisticated null power redistribution scheme was described. In the waterfilling scheme, null power is systematically allocated towards subcarriers with the highest number of bits gained per unit of null power received. Simulation results showed that the waterfilling scheme yielded a higher data rate increase for the same number of nulls compared to the simple null power reallocation scheme. If implemented in an FPGA and tested with the WiGLAN nodes, the estimated data rate improvement due to the waterfilling scheme would be 13.2% for approximately 8 nulls.

5.2 Future Work

Besides actual implementation of the current waterfilling scheme in hardware and testing with the WiGLAN nodes to verify a higher average data rate improvement, the current waterfilling scheme can be further simulated and optimized. Many studies such as [3], [4], and [15] have examined optimal ways to distribute a limited amount of transmit power to achieve the highest data rate given a BER constraint and various channel conditions. Additionally, low-complexity implementations of these waterfilling algorithms have been developed by [1], [16], and [17]. These algorithms could be considered for the WiGLAN nodes and implemented in the hardware to obtain measurements of their real-time performance.

Besides adapting the transmit power and modulation scheme, other parameters of a multicarrier system such as its symbol transmission rate, coding rate and coding scheme could also be considered when trying to achieve the highest possible data rate [15]. For example, the length of the cyclic prefix in a symbol could be adjusted based on the channel conditions. Currently in the WiGLAN, the length of the cyclic prefix is set to guard against the worst case maximum excess delay of 70 ns for a channel with a maximum link distance of 10 meters [6]. For a shorter link distance, the multipath spread becomes much smaller, and thus the cyclic prefix length could be reduced to further increase the the data rate.

Finally, the WiGLAN system is designed to study the performance of variable data rate applications such as file transfer, where the highest possible rate is desired. For delay sensitive services such as voice or video that are usually provided at a fixed rate, it is sometimes desirable to optimize over the BER metric instead [2]. Optimization over BER instead of data rate leads to differences in the algorithms. For example, [2] shows that the optimal transmit power allocation when optimized over BER behaves as normal waterfilling under bad channel conditions, but deviates from normal waterfilling performance under good channel conditions. Future work could involve implementing a transmit power waterfilling scheme that optimizes over BER instead of data rate, and assessing the performance of the scheme in hardware.

Appendix A

Simple Power Reallocation Simulation Results

Location	locN	locI	locJ-1	locK	locL	locC	locD	locE	locF	locM	locA	locFG	locN-2	locJ-2	Average
Null	3	2	4	9	11	0	13	3	10	2	5	12	4	8	6.142857
Old BPSK	3	10	7	12	14	2	5	6	15	3	11	20	6	12	9
4-QAM	13	28	46	56	50	26	30	52	35	11	22	49	29	34	34.35714
16-QAM	50	47	35	15	17	36	35	28	31	43	36	11	27	36	31.92857
64-QAM	23	5	0	0	0	26	9	3	1	28	18	0	24	2	9.928571
256-QAM	0	0	0	0	0	2	0	0	0	5	0	0	2	0	0.642857
New BPSK	3	10	7	10	12	2	5	6	14	2	11	16	5	11	8.142857
4-QAM	12	27	42	53	50	26	29	51	35	9	21	53	29	33	33.57143
16-QAM	47	48	39	19	19	36	32	29	32	44	35	10	24	37	32.21429
64-QAM	27	5	0	1	0	26	13	3	1	28	20	1	28	3	11.14286
256-QAM	0	0	0	0	0	2	0	0	0	7	0	0	2	0	0.785714
Bits Gained	10	2	8	14	6	0	10	2	3	15	6	6	11	7	7.142857
Bits/Sym(old)	367	284	239	184	182	370	259	240	215	405	307	162	332	236	270.1429
Bits/Sym (new)	377	286	247	198	188	370	269	242	218	420	313	168	343	243	277.2857
Data Rate Impr (%)	2.725	0.704	3.3473	7.609	3.297	0	3.861	0.833	1.3953	3.704	1.9544	3.704	3.313	2.966	2.815182

Appendix B

Simple Power Reallocation Hardware Results

Trial	Location	Dist from RX (m)	Subtrial	Bits/OFDM	# Syms Saved	Total Bits	BER
1	A	1.51	1	332	1579	524228	0.00023463
2	A	1.51	2	339	1546	524094	0.000057242
3	A	1.51	3	241	2175	524175	3.8155E-06
4	A	1.51	4	346	1515	524190	0.00031668
5	A	1.51	5	332	1579	524228	0.00023463
6	B	5.45	1	187	2803	524161	0.000055327
7	B	5.45	2	218	2404	524072	0.000068693
8	B	5.45	3	230	2279	524170	0.00016216
9	B	5.45	4	254	2064	524256	9.5373E-06
10	B	5.45	5	200	2621	524200	0.000061045
11	B	5.45	6	202	2595	524190	0
12	B	5.45	7	245	2139	524055	0
13	C	4.25	1	236	2221	524156	0.000024802
14	C	4.25	2	256	2047	524032	0.000022899
15	C	4.25	3	244	2148	524112	0.000005724
16	C	4.25	5	275	1906	524150	0.000024802
17	C	4.25	7	258	2032	524256	0
18	C	4.25	8	257	2039	524023	0.00013549
19	D	6.35	1	253	2072	524216	0
20	D	6.35	2	282	1859	524238	0
21	D	6.35	3	212	2472	524064	9.5408E-06
22	D	6.35	4	227	2309	524143	0.00008967
23	D	6.35	5	246	2131	524226	0.000045782
24	D	6.35	7	236	2221	524156	0.00001717
25	D	6.35	8	246	2131	524226	9.5379E-06
26	E	5.35	1	228	2299	524172	1.9078E-06
27	E	5.35	3	162	3236	524232	0.000041966
28	E	5.35	4	231	2269	524139	7.6316E-06
29	E	5.35	5	230	2279	524170	5.7233E-06
30	E	5.35	6	247	2122	524134	0.00004579
31	E	5.35	8	184	2849	524216	1.9076E-06
32	F	5.74	2	239	2193	524127	0
33	F	5.74	4	186	2818	524148	0.000013355
34	F	5.74	6	213	2461	524193	0
35	F	5.74	7	226	2319	524094	1.9081E-06
36	F	5.74	8	251	2088	524088	0.000024805
37	G	3.79	1	328	1598	524144	0.000020987
38	G	3.79	2	275	1906	524150	5.7236E-06
39	G	3.79	3	311	1685	524035	3.8165E-06
40	G	3.79	4	335	1564	523940	0.000019086
41	G	3.79	5	300	1747	524100	0
42	G	3.79	6	334	1569	524046	3.8165E-06
43	G	3.79	7	306	1713	524178	0.000036247
44	G	3.79	8	267	1963	524121	0.000017172
		Overall Average:		254.704545	2126.477273	524146.5	4.18414E-05
		Standard Deviation:		46.8354763	391.9845446	70.85014	7.03032E-05
		1 std dev above avg:		301.540022	2518.461817	524217.3	0.000112145
		1 std dev below avg:		207.869069	1734.492728	524075.6	-2.8462E-05

		New Modulation					
Bits gained	Data rate increase (%)	Nulls	BPSK	4QAM	16QAM	64QAM	256QAM
5	1.53	8	2	23	35	24	0
10	3.04	3	1	27	42	18	1
3	1.26	3	3	57	25	4	0
4	1.17	2	0	30	41	15	4
5	1.22	8	2	23	35	24	0
21	12.65	20	1	49	22	0	0
13	6.34	13	2	46	31	0	0
8	3.6	6	4	51	31	0	0
6	2.42	4	4	43	41	0	0
24	13.64	17	4	44	27	0	0
25	14.12	15	2	50	25	0	0
4	1.66	4	5	46	37	0	0
4	1.72	6	4	48	34	0	0
22	9.4	12	4	26	50	0	0
17	7.49	9	2	42	38	1	0
9	3.38	6	1	34	50	1	0
11	4.45	9	2	34	47	0	0
16	6.64	10	3	31	48	0	0
0	0	2	5	46	39	0	0
6	2.17	3	0	37	52	0	0
8	3.92	13	4	47	27	1	0
10	4.61	16	3	34	39	0	0
2	0.82	8	2	43	38	1	0
5	2.16	13	2	40	34	3	0
3	1.23	7	2	44	39	0	0
8	3.64	4	4	56	28	0	0
14	9.46	12	8	67	5	0	0
5	2.21	4	1	60	26	1	0
4	1.77	5	2	56	29	0	0
6	2.68	4	3	48	37	0	0
7	3.95	7	4	72	9	0	0
12	5.29	7	3	46	36	0	0
31	20	30	0	32	29	1	0
7	3.4	19	1	38	34	0	0
13	6.1	16	4	33	39	0	0
6	2.45	8	7	33	43	1	0
9	2.82	3	2	39	20	28	0
6	2.23	1	3	50	28	10	0
8	2.64	7	1	29	39	16	0
6	1.82	2	3	35	25	27	0
2	0.67	1	2	43	32	14	0
19	6.03	7	2	19	45	19	0
1	0.33	1	2	35	45	9	0
12	4.71	10	1	35	40	6	0
9.477272727	4.382727273	8.295455	2.659091	41.38636	34.45455	5.090909	0.113636
6.999962247	4.169656371	6.063921	1.683617	11.51383	9.940414	8.539425	0.618171
16.47723497	8.552383643	14.35938	4.342708	52.90019	44.39496	13.63033	0.731807
2.47731048	0.213070902	2.231533	0.975474	29.87254	24.51413	-3.448516	-0.504535

Old Modulation

Nulls	BPSK	4QAM	16QAM	64QAM	256QAM	Total Data Carriers
8	3	22	37	22	0	92
3	1	30	40	18	0	92
3	4	57	24	4	0	92
2	0	31	40	16	3	92
8	3	22	37	22	0	92
20	6	52	14	0	0	92
13	5	48	26	0	0	92
6	6	52	28	0	0	92
4	4	46	38	0	0	92
17	8	50	17	0	0	92
15	7	55	15	0	0	92
4	5	48	35	0	0	92
6	4	50	32	0	0	92
12	6	34	40	0	0	92
9	5	45	33	0	0	92
6	2	37	46	1	0	92
9	3	38	42	0	0	92
10	7	33	42	0	0	92
2	5	46	39	0	0	92
3	0	40	49	0	0	92
13	6	47	26	0	0	92
16	7	33	36	0	0	92
8	2	44	37	1	0	92
13	5	38	33	3	0	92
7	3	44	38	0	0	92
4	4	60	24	0	0	92
12	14	65	1	0	0	92
4	2	61	24	1	0	92
5	2	58	27	0	0	92
4	3	51	34	0	0	92
7	5	74	6	0	0	92
7	3	52	30	0	0	92
30	9	33	20	0	0	92
19	6	34	33	0	0	92
16	7	35	34	0	0	92
8	7	36	40	1	0	92
3	3	38	24	24	0	92
1	3	51	29	8	0	92
7	1	30	41	13	0	92
2	3	36	26	25	0	92
1	2	44	31	14	0	92
7	3	20	50	12	0	92
1	3	34	45	9	0	92
10	3	36	39	4	0	92
8.295455	4.318182	42.95455	31.86364	4.5	0.068182	
6.063921	2.594921	11.76308	10.60187	7.711363	0.452267	
14.35938	6.913103	54.71762	42.4655	12.21136	0.520449	
2.231533	1.723261	31.19147	21.26177	-3.211363	-0.384085	

Appendix C

Waterfilling Power Reallocation Simulation Results

Location	locN	locI	locJ-1	locK	locL	locB	locC	locD	locE	locF	locM	locA	locFG	locN_2	locJ-2	Average
Nulls Count	3	2	4	9	11	4	0	13	3	10	2	5	12	4	8	5.85714
I_Count	24	12	23	20	12	23	22	21	11	13	28	16	11	20	19	48.5
II_Count	24	28	22	23	27	20	28	21	21	22	26	23	22	20	24	23.3571
III_Count	16	16	12	10	10	17	16	11	14	12	9	14	12	14	8	13.0714
II_non-BPSK	23	22	16	16	18	15	27	19	17	14	24	17	10	15	16	18.0714
II_BPSK	1	6	6	7	9	5	1	2	4	8	2	6	12	5	8	5.28571
I_Select	6	4	8	18	12	8	0	21	6	13	4	10	11	8	16	9.21429
II_Select	0	0	0	0	5	0	0	2	0	3	0	0	6	0	0	1.14286
III_Select	0	0	0	0	0	0	0	0	0	0	0	0	0	0	0	0
II_non-BPSK	0	0	0	0	5	0	0	2	0	3	0	0	6	0	0	1.14286
II_BPSK	0	0	0	0	0	0	0	0	0	0	0	0	0	0	0	0
Bits/Sym (new)	379	292	255	220	216	333	370	305	252	247	413	327	196	348	268	296.643
Bits/Sym (old)	367	284	239	184	182	317	370	259	240	215	405	307	162	332	236	275.929
Bits gained	12	8	16	36	34	16	0	46	12	32	8	20	34	16	32	20.7143
Data Rate Impr (%)	3.27	2.817	6.695	19.57	18.68	5.05	0	17.76	5	14.9	1.98	6.51	20.99	4.819	13.56	9.14402
256-QAM - region 1	0	0	0	0	0	0	2	0	0	0	5	0	0	2	0	0.64286
64-QAM - region 2	0	0	0	0	0	0	0	0	0	0	3	1	0	0	0	0.28571
64-QAM - region 3	0	0	0	0	0	0	0	0	0	0	0	0	0	0	0	0
64-QAM - region 4	0	0	0	0	0	0	0	0	0	0	0	0	0	0	0	0
64-QAM - region 5	23	5	0	0	0	12	26	9	3	1	25	17	0	24	2	10.3571
16-QAM - region 6	6	2	0	1	2	8	0	11	3	4	1	4	3	2	2	3.35714
16-QAM - region 7	0	0	0	0	2	0	0	2	0	0	0	0	0	0	0	0.28571
16-QAM - region 8	0	0	0	0	0	0	0	0	0	0	0	0	0	0	0	0
16-QAM - region 9	44	45	35	14	13	42	36	22	25	27	42	32	8	25	34	29.2857
4-QAM - region 10	0	2	8	17	10	0	0	10	3	9	0	5	8	6	14	5.57143
4-QAM - region 11	0	0	0	0	3	0	0	0	0	3	0	0	6	0	0	0.85714
4-QAM - region 12	0	0	0	0	0	0	0	0	0	0	0	0	0	0	0	0
4-QAM - region 13	13	26	38	39	37	19	26	20	49	23	11	17	35	23	20	26.8571
BPSK - region 14	0	0	0	0	0	0	0	0	0	0	0	0	0	0	0	0
BPSK - region 15	3	10	7	12	14	7	2	5	6	15	3	11	20	6	12	8.64286
Null - region 16	31	30	32	37	39	32	28	41	31	38	30	33	40	32	36	33.8571
Num Pilots	8	8	8	8	8	8	8	8	8	8	8	8	8	8	8	8
Total Subcarriers	128	128	128	128	128	128	128	128	128	128	128	128	128	128	128	128

Bibliography

[1] Kannan Ramchandran Brian Krongold and Douglas Jones. Computationally efficient optimal power allocation algorithms for multicarrier communication systems. *IEEE Transactions on Communications*, 48(1):23–27, 2000.

[2] Chang Soon Park and Kwang Bok Lee. Transmit power allocation for ber performance improvement in multicarrier systems. *IEEE Transactions on Communications*, 52(10):1658–1663, 2004.

[3] Kwang Bok Lee Jiho Jang and Yong-Hwan Lee. Frequency-time domain transmit power adaptation for a multicarrier system in fading channels. *IEEE Transactions on Communications*, pages 100–103, 2001.

[4] Andrea Goldsmith and Soon-Ghee Chua. Variable-rate variable-power mqam for fading channels. *IEEE Transactions on Communications*, 45(10):1218–1230, 1997.

[5] Farinaz Edalat et. al. Measured data rate from adaptive modulation in wideband ofdm systems. In *IEEE International Conference on Ultra-Wideband*, 2006.

[6] Jit Ken Tan. An adaptive orthogonal frequency division multiplexing baseband modem for wideband wireless channels. Master's thesis, Massachusetts Institute of Technology, May 2006.

[7] John Terry and Juha Heiskala. *OFDM Wireless LANs: A Theoretical and Practical Guide*. SAMS, Second edition, 2002.

[8] Theodore Rappaport. *Wireless Communications: Principles and Practice.* Prentice Hall, 1996.

[9] Jose Tellado. *Multicarrier Modulation with Low PAR: Applications to DSL and Wireless.* Kluwer Academic Publishers, 2000.

[10] Marc Engels. *Wireless OFDM Systems: How to make them work?* Kluwer Academic Publishers, 2002.

[11] L Hanzo et. al. *Single- and Multi-carrier Quadrature Amplitude Modulation.* John Wiley and Sons, 2000.

[12] Nir Matalon. An implementation of a 5.25ghz transceiver for high data rate wireless applications. Master's thesis, Massachusetts Institute of Technology, July 2005.

[13] Michael Speth et. al. Optimum receiver design for wireless broad-band systems using ofdm - part 1. *IEEE Transactions on Communications*, 1999.

[14] Michael Pursley. *Introduction to Digital Communications.* Prentice Hall, 2005.

[15] Seong Taek Chung and Andrea Goldsmith. Degrees of freedom in adaptive modulation: A unified view. *IEEE Transactions on Communications*, 2001.

[16] Wei Yu and John Cioffi. Constant-power waterfilling: Performance bound and low-complexity implementation. *IEEE Transactions on Communications*, 54(1):23–28, 2006.

[17] David Dardari. Ordered subcarrier selection algorithm for ofdm-based high-speed wlans. *IEEE Transactions on Wireless Communications*, 3(5):1452–1458, 2004.